Frontiers in Health Informatics
ISSN-Online: 2676-7104
www.healthinformaticsjournal.com
2024; Vol 13: Issue 8
Open Access

Formulation, Optimization and Characterization of Fluconazole Loaded Ethosomal and Liposomal Vesicular Systems for Transdermal Drug Delivery

Apoorva Tiwari*, Sachin K. Jain[1], Sudha Vengurlekar[1]

*Research Scholar, Faculty of Pharmacy, Oriental University Indore, MP 453555

[1]Faculty of Pharmacy, Oriental University Indore, MP 453555

Corresponding Author –

apoorvatiwari2010@gmail.com.

Cite this paper as: Apoorva Tiwari, Sachin K. Jain, Sudha Vengurlekar (2024) Formulation, Optimization and Characterization of Fluconazole Loaded Ethosomal and Liposomal Vesicular Systems for Transdermal Drug Delivery..*Frontiers in Health Informatics*, *Vol.13, No.8*, 8194-8216

ABSTRACT:

Transdermal drug delivery systems (TDDS) have emerged as an effective alternative to conventional drug administration routes by overcoming limitations such as first-pass metabolism, fluctuating plasma drug concentration, and poor patient compliance. However, the barrier property of the stratum corneum restricts the permeation of many therapeutic agents through the skin. Vesicular carriers such as ethosomes and liposomes have demonstrated significant potential in enhancing transdermal permeation and improving therapeutic efficacy. The present study was aimed at the formulation, optimization, and characterization of fluconazole-loaded ethosomal and liposomal vesicular systems for enhanced transdermal delivery. Ethosomes were prepared by a modified hot method, while liposomes were prepared using the thin film hydration technique. Optimization of the formulations was carried out using a Taguchi Design of Experiments (DoE) approach. Vesicle size and entrapment efficiency were selected as the major response variables for optimization. The prepared ethosomal formulations exhibited vesicle sizes ranging from 161.08 ± 3.214 nm to 552.82 ± 1.254 nm with entrapment efficiency ranging from 64.08 ± 1.213% to 90.83 ± 1.241%. Among all batches, formulation TE4 showed the smallest vesicle size of 161.08 ± 3.214 nm, whereas formulation TE2 exhibited maximum entrapment efficiency of 90.83 ± 1.241%. The optimized ethosomal formulation EF2 showed vesicle size of 368.4 nm and entrapment efficiency of 85.50%. Similarly, liposomal formulations demonstrated vesicle sizes ranging from 126.79 ± 1.175 nm to 510.13 ± 1.154 nm and entrapment efficiency ranging from 55.12 ± 1.241% to 91.70 ± 1.029%. Formulation TL4 exhibited the minimum vesicle size of 126.79 ± 1.175 nm, while formulation TL6 showed maximum entrapment efficiency of 91.70 ± 1.029%. Response surface analysis confirmed that phospholipid concentration and ethanol content significantly influenced vesicle size and drug entrapment. The study demonstrated that optimized ethosomal and liposomal vesicular systems possess suitable physicochemical characteristics for effective transdermal delivery of fluconazole and may serve as promising carriers for enhanced antifungal therapy.

Keywords: Liposomal,Ethosomes, Transdermal drug delivery systems (TDDS), fluconazole, Response surface analysis..

INTRODUCTION

Transdermal drug delivery systems (TDDS) have gained significant attention as an alternative to conventional oral and parenteral drug delivery due to their ability to avoid first-pass metabolism, provide sustained drug release, and improve patient compliance. However, the stratum corneum acts as a major barrier to drug permeation through the skin, limiting the effectiveness of many therapeutic agents.

Vesicular carrier systems such as liposomes and ethosomes have been widely investigated to enhance transdermal drug delivery. Liposomes are phospholipid vesicles capable of encapsulating both hydrophilic and lipophilic drugs, but their penetration into deeper skin layers is limited. Ethosomes are modified liposomes containing high concentrations of ethanol, which increase vesicle flexibility and improve skin permeation by disrupting the lipid organization of the stratum corneum.

Fluconazole is a broad-spectrum antifungal drug used in the treatment of fungal infections. Conventional oral therapy is associated with adverse effects such as hepatotoxicity and gastrointestinal disturbances, while topical formulations show inadequate skin penetration. Therefore, development of vesicular transdermal systems may improve drug permeation, enhance therapeutic efficacy, and reduce systemic side effects..

In the present study, fluconazole-loaded ethosomal and liposomal formulations were prepared and optimized using Design of Experiments (DoE) based Taguchi design. The study aimed to develop optimized vesicular systems with desirable vesicle size and high entrapment efficiency for effective transdermal delivery of fluconazole.

MATERIALS AND METHODS

Materials Used in Investigation

Fluconazole was obtained as a gift sample from Modern Laboratories, Indore. Soya phosphatidylcholine, cholesterol, ethanol, chloroform, methanol, Carbopol 934, triethanolamine, and other analytical grade chemicals and solvents were used throughout the investigation.

Preformulation Studies of Fluconazole

Preformulation studies constitute a systematic evaluation of the physicochemical properties of a drug substance prior to its incorporation into a formulation development program. The intrinsic properties of the drug significantly influence processing considerations, including the method of preparation, encapsulation efficiency, excipient compatibility, and the pharmacokinetic behavior of the resulting dosage form. Preformulation investigations are therefore considered essential for the rational development of safe, efficacious, and stable pharmaceutical products.

- The physiochemical properties of drug, and an assessment of their relevance to the final formulation.
- The chemical and physical stability of drug.
- Chemical /physical compatibility of the active with potential excipients.

Physical appearance: The fluconazole drug substance was subjected to organoleptic evaluation, encompassing assessment of color, taste, and odor.

Determination of Wavelength Maxima (λ_{max}): A stock solution was prepared by dissolving 10 mg of accurately weighed fluconazole in 100 ml of ethanol. An aliquot of 1 ml was transferred to a 10 ml volumetric flask and the volume was adjusted to the mark with ethanol. This solution was scanned across a wavelength range of 200–400 nm using a double-beam UV/Vis spectrophotometer. An identical procedure was applied for the determination of λ_{max} in phosphate buffer pH 7.4.

Preparation of calibration curve of fluconazole

Calibration curve in phosphate buffer pH 7.4: Fluconazole (10 mg, accurately weighed) was dissolved in 5 ml methanol and the volume made up to 100 ml with phosphate buffer pH 7.4 in a volumetric flask. A 1 ml aliquot was transferred to a 10 ml volumetric flask and diluted with the same buffer to yield a working stock concentration of 10 µg/ml. Serial dilutions of 1–10 ml from this stock were transferred to individual 10 ml volumetric flasks and made up to volume with phosphate buffer pH 7.4. Absorbances were recorded at 260 nm against a phosphate buffer blank. A calibration curve was constructed by plotting absorbance versus concentration, and the line of best fit was derived by linear regression.

Calibration curve in ethanol: UV scanning of fluconazole in the 200–400 nm range using a Shimadzu-1700 spectrophotometer identified the wavelength of maximum absorbance at 260 nm. For calibration, 10 mg of accurately weighed fluconazole was dissolved in 5 ml ethanol and the volume adjusted to 100 ml with ethanol in a volumetric flask. A 1 ml aliquot was diluted to 10 ml with ethanol to prepare a 10 µg/ml stock. Serial aliquots of 1–10 ml were prepared in 10 ml volumetric flasks and made up to volume with ethanol. Absorbance measurements were taken at 260 nm against an ethanol blank, and the calibration curve was plotted as absorbance against concentration.

FTIR Spectra of fluconazole: Infrared spectra of drug-excipient physical mixtures were acquired using the potassium bromide (KBr) disc technique on a Fourier Transform Infrared Spectrophotometer. Baseline correction was performed using a blank KBr pellet. Sample pellets of approximately 1 mm diameter were prepared by mixing 3–5 mg of the drug-excipient mixture with 100–150 mg KBr and compressing under a hydraulic press. The pellet was placed in the instrument sample compartment and scanned over the wavenumber range of 400–4000 cm^{-1}.

Melting point determination by DSC: Melting point is an established indicator of drug purity; chemically pure substances exhibit sharp, well-defined melting points, while pharmaceutical-grade compounds, which may contain minor impurities or polymorphic forms, often display a characteristic melting range. Melting point was determined by differential scanning calorimetry (DSC) following the method of Kalaiselan et al. (2006). Samples of 2–4 mg were placed in non-hermetically sealed aluminum pans and heated at a scan rate of 5°C/min over a temperature range of 50–200°C. The resulting DSC thermograms were analyzed to determine the melting behavior of fluconazole.

pH measurement: Solution pH was determined using a calibrated digital pH meter. For this purpose, 1 g of fluconazole was accurately weighed, dissolved in 5 ml ethanol, and the volume was brought to 100 ml with distilled water under sonication. The resulting solution was filtered, and the pH of the filtrate was recorded.

Flow properties: Powder flow characteristics were assessed through measurement of the angle of repose, Carr's compressibility index, and Hausner's ratio.
To determine the angle of repose, the powder was allowed to flow freely through a fixed funnel positioned with its lower tip exactly 2.0 cm above a flat surface. Powder was added until the apex of the resulting cone contacted the funnel tip. The angle of repose (θ) was calculated as the inverse tangent of the ratio of cone height to base radius (Alanzi, 2007; Carstensen and Chan, 1977).
For bulk and tapped density measurements, powder was carefully poured through a funnel into a graduated cylinder to the 10 ml mark. Excess material was leveled with a spatula and the cylinder weight was recorded. The cylinder was then mechanically tapped from a height of 2.0 cm until no further volume reduction occurred.
Bulk density (ρb) and tapped density (ρt) were calculated, and Hausner's ratio (HR) and Carr's index (IC) were derived using the standard equations.

$$H_R = \frac{\rho_t}{\rho_b}$$

$$I_C = \frac{(\rho_t - \rho_b)}{\rho_t} \times 100$$

Table 1: Angle of repose, carr's index and hausner ratio (Staniforth and Aulton 2007).

Angle of Repose	Carr's Index	Hausner Ratio	Type of Flow
20°	- 5%		xcellent
)–30°	2– 6%	1.25	ood
)–40°	3–21%		Fair to passable
	3– 5%	1.25	oor
	3–38%	25–1.5	ery poor
	40%		xtremely poor

Solubility study: The equilibrium solubility of fluconazole was evaluated in distilled water, 0.1N hydrochloric acid, ethanol, methanol, chloroform, acetone, DMSO, and various buffer systems at pH 1.2, 2.5, 5.0, 7.4, 9.0, and 10.0, all at 25 ± 2°C. An excess quantity of drug was added to 5 ml of each solvent in screw-capped glass vials, and the vials were mechanically agitated at 25°C for 48 hours to achieve dissolution equilibrium. The resulting suspensions were filtered through 0.45 µm membrane filters, and the drug concentration in the filtrate was determined spectrophotometrically.

Determination of partition coefficient: The partition coefficient is defined as the equilibrium ratio of the unionized drug concentration between an organic phase and an aqueous phase, and is conventionally expressed on a logarithmic scale as log P. This parameter provides a quantitative measure of lipophilicity. A log P of 0 indicates equal distribution between the two phases; positive values indicate preferential partitioning into the organic phase, while negative values indicate hydrophilicity. For example, a log P of +5 indicates 100,000-fold greater solubility in the organic phase, whereas a log P of −2 indicates 100-fold greater affinity for water.

$$log\ P_{oct/wat} = log\left(\frac{[solute]_{octanol}}{[solute]^{un-ionized}_{water}}\right)$$

The partition coefficient was determined using n-octanol as the organic phase and phosphate buffer pH 7.4 as the aqueous phase. Equal volumes of both phases were combined and mutually saturated by shaking on a mechanical water bath at 37 ± 2°C for 24 hours, followed by phase separation via centrifugation at 2000 rpm. Equal aliquots of the pre-saturated phases were then placed in individual conical flasks, and 100 mg of drug was added to each. Partitioning was allowed to proceed for 6 hours with shaking at 100 rpm and 37 ± 2°C. The phases were then separated by centrifugation at 1000 rpm for 5 minutes, and drug content in each phase was quantified spectrophotometrically (Martin et al., 1983; Leo et al., 1971).
Loss on drying: Moisture content was directly quantified using an infrared moisture balance. Fluconazole (5.0 g) was weighed and subjected to drying at 100–105°C for 5 minutes, and the percentage loss on drying was calculated from the change in mass.
Drug–Excipient compatibility study: DSC thermograms of the drug, excipients, and their physical mixtures were recorded using a differential scanning calorimeter. Samples of 5–10 mg were accurately weighed and

hermetically sealed in flat-bottomed aluminum pans. Heating was conducted over the temperature range of 50–400°C under a nitrogen atmosphere (200 ml/min) at a constant rate of 10°C/min, with alumina used as the reference material.

Preparation of Ethosomes: Ethosomes were prepared by a modified hot method based on US patent 5,540,934 (1995), utilizing a magnetic stirrer, probe sonicator, and high-pressure homogenizer. The composition involved 10 mg fluconazole, 1–5% w/v SPC, 20–50% w/v ethanol, 10–20% w/v propylene glycol, and water to 100%. The drug was dissolved in the ethanol–propylene glycol mixture, then added to an aqueous phospholipid dispersion maintained at 40°C with continuous stirring. The mixture was probe-sonicated for 5 minutes between each processing cycle. The resulting dispersion was homogenized at 15,000 psi for three cycles using a high-pressure homogenizer to yield nano-sized ethosomes (Touitou et al., 1996).

Screening of influential variables: A Taguchi orthogonal array design was adopted to identify the formulation and process variables most significantly influencing ethosomal performance. Table 2 details the high and low levels assigned to each variable evaluated for its contribution to ethosome characteristics.

Table 2 List of variables employed in Taguchi Screening Study

Factors	Levels	
	Low (-1)	High (+1)
Amount of SPC (%w/v)	1	5
Amount of Ethanol (%w/v)	20	50
Amount of Propylene Glycol (%w/v)	10	20

Table 3 presents the L8 orthogonal array for the three-factor, two-level Taguchi design used in this study. Vesicle size and entrapment efficiency were selected as the primary response variables for identifying the most influential formulation factors.

Table 3 Composition of ethosome on the basis of Taguchi Screening Design

Run	B. No	SPC (%w/v)	Ethanol (%w/v)	Propylene Glycol (%w/v)
1	TE1	5	20	20
2	TE2	1	20	10
3	TE3	1	50	10
4	TE4	5	50	10
5	TE5	1	50	20
6	TE6	1	20	20
7	TE7	5	50	20
8	TE8	5	20	10

Preparation of Ethosomes

Ethosomal formulations were prepared using modified hot method. Required quantities of phospholipid and cholesterol were dissolved in ethanol under continuous stirring. Fluconazole was added to the ethanolic phase followed by addition of distilled water maintained at suitable temperature. The formulation was stirred continuously to obtain vesicular dispersion and sonicated to reduce vesicle size.

Different ethosomal formulations were prepared by varying concentrations of phospholipid and ethanol according to Taguchi screening design. Optimization was carried out using Design of Experiments (DoE) approach to obtain formulations with minimum vesicle size and maximum entrapment efficiency.

Table 4: Composition of optimized ethosome formulation

Formulation	SPC (%w/v)	Ethanol (%w/v)	Propylene Glycol (%w/v)
EF1	3	43	10

Preparation of Liposomes

The liposomal suspension was transferred to a 10 ml centrifuge tube, diluted to 5 ml with distilled water, and centrifuged at 2000 rpm for 20 minutes to remove undissolved drug. An appropriate volume of protamine solution was added to the cleared supernatant and allowed to react for 10 minutes, causing liposomal aggregation. The aggregated liposomes were collected by ultracentrifugation at 15,000 rpm for 20 minutes. Supernatant and sediment were separated and their volumes recorded. The sediment was diluted with distilled water to 5 ml, and drug concentrations in both fractions were determined spectrophotometrically to calculate the entrapped and unentrapped drug contents (Bendas et al., 2008).

Table 5 Composition of optimized liposome formulation

Formulation	Lecithin (mg)	Cholesterol (mg)	Speed (rpm)
LF2	152	38.3	100

RESULT AND DISCUSSION

Preformulation Studies

Organoleptic evaluation: Visual and sensory examination of the drug powder revealed that fluconazole presented as a white to off-white crystalline powder with no characteristic odor.

Table 6: Organoleptic property of fluconazole

Color	White to off white powder
Odor	Odorless
Taste	Tasteless

Determination of wavelength maxima in phosphate buffer pH 7.4: A UV spectrophotometric analytical method was developed for quantitative estimation of fluconazole, offering sensitivity, accuracy, and reproducibility. The method was designed to provide reliable and rapid determination of drug concentration.
UV absorption analysis of fluconazole in phosphate buffer pH 7.4 indicated maximum absorbance at 260 nm (Figure 5.1). A linear Beer-Lambert relationship was established with a correlation coefficient of 0.997 across a concentration range of 10–50 µg/ml. The three-dimensional absorption spectra are presented in Figure 1

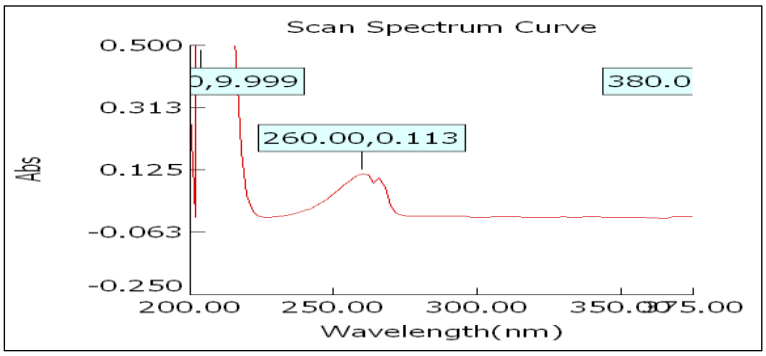

Figure 1 Wavelength maxima of fluconazole in phosphate buffer pH 7.4.

Determination of wavelength maxima in ethanol: The maximum UV absorbance of fluconazole dissolved in ethanol was observed at 260 nm (Figure 5.3). The drug exhibited a linear relationship between concentration and absorbance, with a correlation coefficient of 0.998 over the range of 10–50 µg/ml. Three-dimensional spectra in ethanol are illustrated in Figure 2

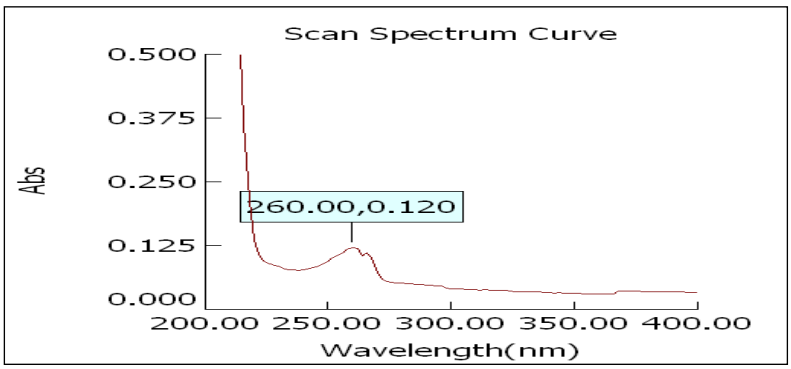

Figure 2: Wavelength maxima of fluconazole in ethanol

Calibration curve of fluconazole in phosphate buffer pH 7.4 and ethanol : Standard calibration curves were constructed by plotting absorbance against known drug concentrations. The regression coefficients (r^2) were determined to be 0.997 in phosphate buffer pH 7.4 and 0.998 in ethanol (Table 5.2), with statistical parameters

detailed in Table 5.3. A linear concentration–absorbance relationship was confirmed over the range of 10–50 µg/ml in both media (Figures 3 and 4).

Table 7: Calibration curve points of the proposed method for the estimation of fluconazole.

Conc. (µg/ml)	Phosphate buffer pH 7.4 Absorbance* (260nm)	Ethanol Absorbance*(260nm)
10	0.110±0.002	0.075±0.001
20	0.210±0.001	0.169±0.002
30	0.325±0.002	0.281±0.001
40	0.425±0.001	0.398±0.002
50	0.556±0.001	0.510±0.001

*Average of three readings

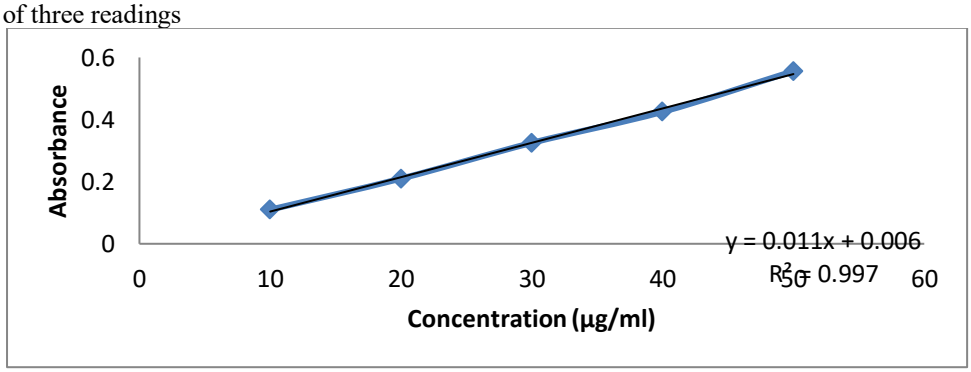

Figure 3: Calibration curve of fluconazole in phosphate buffer pH 7.4 at 260 nm

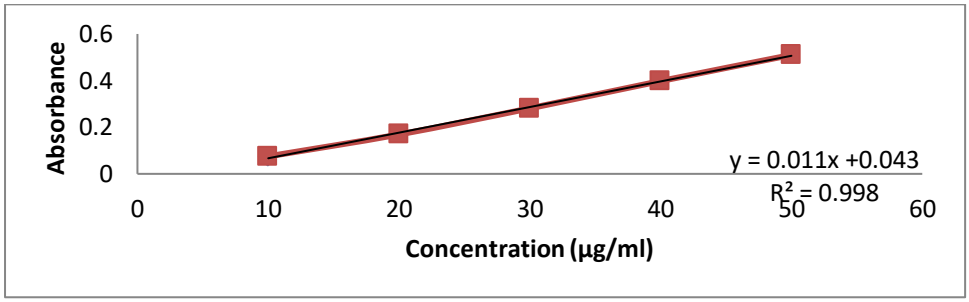

Figure 4 : Calibration curve of fluconazole in ethanol at 260 nm

Table: 8: Statistical parameters related to standard curve of fluconazole at 260 nm

Media	Parameters	Values
Phosphate buffer pH 7.4	Beer's Law Range	10-50µg/ml
	Regression Coefficient	$R^2 = 0.997$
	Regressed line equation (y = mx + c)	y = 0.011x + 0.006
Ethanol	Beer's Law Range	10-50µg/ml
	Regression Coefficient	$R^2 = 0.998$
	Regressed line equation (y = mx + c)	y = 0.011x + 0.043

Where y is the response, x is the concentration, m is the slope and c is the intercept of a best fit line to the data.

Fourier-Transform Infra Red Spectroscopy (FTIR): The structural identity of the drug was confirmed through FTIR analysis. Diagnostic absorption peaks corresponding to the functional groups of fluconazole were identified and recorded. The characteristic peaks are depicted in Figure 5 and their corresponding wave numbers are listed in Table 5.4.

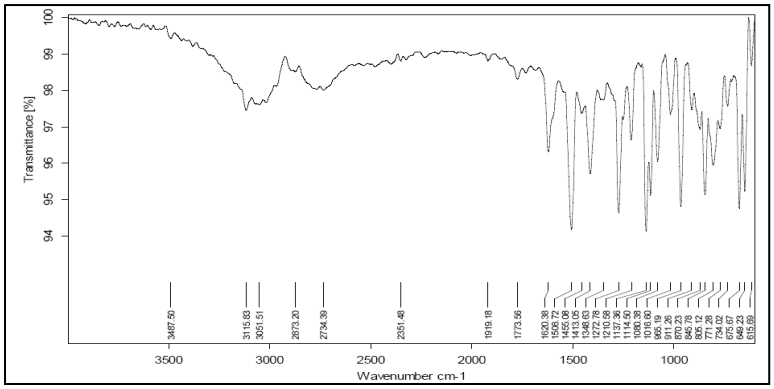

Figure 5 FT-IR of fluconazole

Table 9: Major peaks observed in the FTIR spectrum

Bands	Wave number(cm-1)
OH Streching	3487.50
CH2 Stretching	3115.83
C=C stretching vibration	1620.38
CH2 scissor stretching vibration	1413.05
C-C stretching vibration	1114.50
C - F Stretch	870.23

Changes in peak position or intensity in FTIR spectra are indicative of molecular interactions such as hydrogen bonding. The FTIR spectrum of fluconazole displayed a prominent absorption band at 3487.50 cm^{-1} attributable to O–H stretching, and a band at 3115.83 cm^{-1} corresponding to C–H stretching. In the 2,4-difluorobenzyl moiety, a C=C stretching vibration was observed at 1620.38 cm^{-1}. Additional peaks at 1413.05 cm^{-1} and 1114.50 cm^{-1} were assigned to CH_2 scissoring and C–C stretching vibrations, respectively.

Comparison of the obtained FTIR data with reference spectra from Sakharam et al. (2012) demonstrated agreement in the positions of functional group peaks, thereby confirming the purity and authenticity of the fluconazole sample.

Melting point determination: Melting point analysis serves as a primary indicator of sample purity, since even trace impurities can cause a measurable depression or broadening of the melting range. The experimentally determined melting point of fluconazole was 139°C (Figure 5.8), which is in conformity with Indian Pharmacopoeia standards and confirms the purity of the sample.

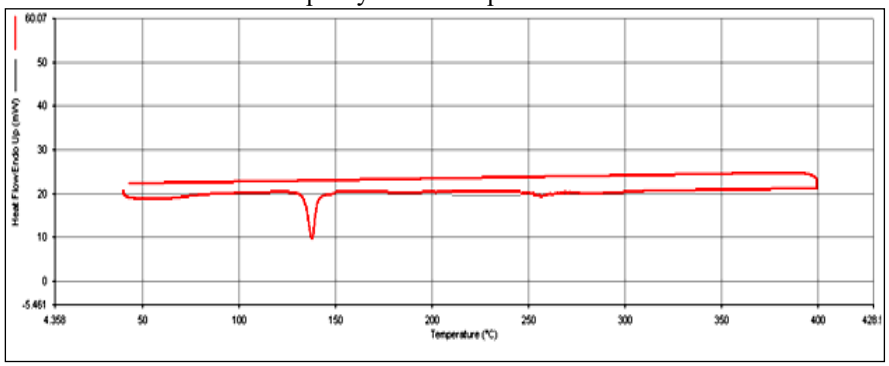

Figure 6: DSC thermogram showing melting point of fluconazole

pH of drug solution: The pH of a 1% w/v aqueous solution of fluconazole was measured using a calibrated digital pH meter and recorded as 7.8 ± 0.002

Flow properties: Bulk density, defined as the mass-to-volume ratio of a powder, is expressed in g/cm^3 and encompasses both the solid particle volume and interparticulate void space. This parameter is significant in the selection and sizing of processing and handling equipment (Jaimini et al., 2007). The measured flow properties of fluconazole API are presented in Table 5.5. A Carr's compressibility index of 53.30%, an angle of repose of 43.56°, and a Hausner's ratio of 1.5 were recorded, collectively indicating poor powder flowability and

compressibility.

Table 10: Flow properties of fluconazole.

Parameter	Fluconazole
Angle of Repose	43.56o
Carr index (%)	53.30
Hausners Ratio	1.5

Solubility studies: The solubility profile of fluconazole was assessed in a range of solvents at ambient temperature (Table 5.6). The drug was found to be freely soluble in ethanol and methanol, soluble in DMSO, acetone, and chloroform, and slightly soluble in 0.1N hydrochloric acid and phosphate buffer pH 7.4. It was essentially insoluble in distilled water.

Table 11: Solubility studies of fluconazole in different solvent

Solvent used	**Solubility(mg/ml)**
Distilled Water	0.001±0.00
0.1 N Hydrochloric acid	11.12±0.22
Ethanol	63.25±0.54
Methanol	47.58±0.78
Chloroform	31.24±0.54
Acetone	21.57±0.43
DMSO	05.24±0.05
Citric acid buffer pH 1.2	30.21±0.54
Citric acid buffer pH 2.5	30.45±0.47
Acetic acid buffer pH 5.0	24.52±0.28
Phosphate buffer pH 7.4	35.24±0.34
Phosphate buffer pH 9.0	18.17±0.12
Phosphate buffer pH 10.0	15.95±0.04

Determination of partition coefficient: The partition coefficient was evaluated using the shake flask method to assess the relative distribution of the drug between aqueous and non-aqueous phases. This measurement facilitates the prediction of drug concentration in each phase. The partition coefficient of fluconazole was determined to be 0.57 ± 0.001, indicating its moderately hydrophobic character.

Loss on drying: The percentage of loss on drying of fluconazole was found to be 0.68±0.013% w/w respectively.

Drug-Excipient compatibility study: DSC analysis of fluconazole showed a characteristic endothermic peak at 139°C. Samples of the drug–cholesterol binary mixture stored under accelerated stability conditions (40°C/75% RH) for 30 days were subjected to DSC analysis. The melting endotherm of fluconazole remained unchanged at 139°C, indicating the absence of any physicochemical interaction between fluconazole and cholesterol (Figures 5.9–5.9c).

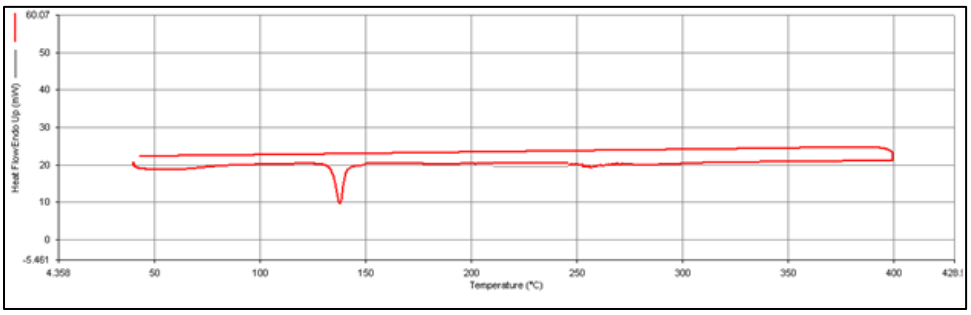

(a)

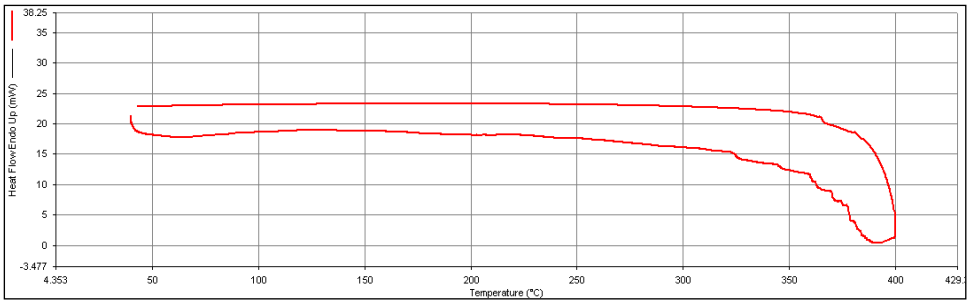

(b)

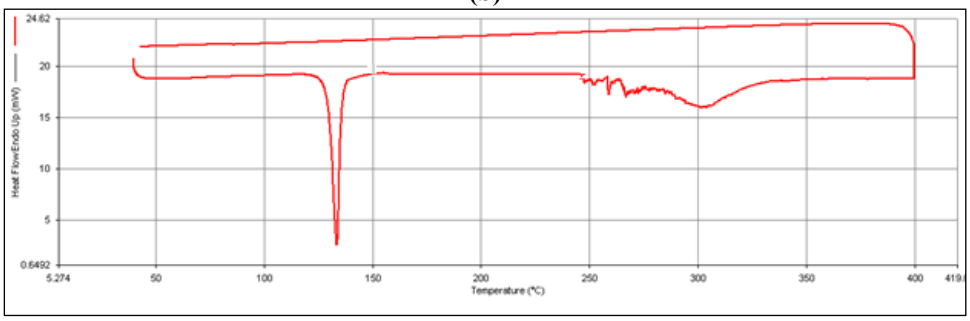

(c)

Figure 7: DSC thermogram of (a) pure drug, (b) cholesterol, (c) drug + cholesterol

Table 12: Comparative data of Preformulation studies

Parameter	Observation
Melting Point	139 ± 1.2oC
pH (1% w/v solution)	7.8±0.002
Angle of repose	43.56 Degree
Compressibility index (%)	53.30±0.05%.
Hausner ratio	1.5±0.001
Solubility of Fluconazole	Freely soluble in Ethanol, Methanol soluble in chloroform, slightly soluble in 0.1N HCl and insoluble in water
Partition coefficient	0.57±0.02
Loss on Drying (%)	0.68 ± 0.013

The results of preformulation characterization (Table 5.7) established that fluconazole is an odorless, white crystalline powder. The drug demonstrated solubility in phosphate buffer pH 7.4, acetone, and 0.1N HCl, with free solubility in methanol and ethanol, and negligible solubility in water. The experimentally determined melting point of 139 ± 2°C was consistent with the Indian Pharmacopoeia reference value of 140°C.

Analysis of the FTIR spectrum of the physical mixture confirmed that the characteristic functional groups of fluconazole were preserved, with no significant shifts or changes in peak intensities. This observation indicates that no chemical reaction occurred between the drug and cholesterol during preparation. DSC studies further corroborated compatibility between the two components. The partition coefficient value of 0.57 in an n-octanol/water system reflected the lipophilic tendency of fluconazole. Collectively, these preformulation data confirmed the feasibility of formulating fluconazole into ethosomal and liposomal vesicular drug delivery systems using appropriate preparation techniques.

Evaluation of Ethosomes: Table 5.8 summarizes vesicle size and entrapment efficiency data for the ethosomal formulations. Vesicle diameters ranged from 161.08 to 552.8 nm, while entrapment efficiency values spanned 63.70 to 90.89%.

Table 13: Evaluations of ethosomal formulations of Taguchi Screening Design

Formulation	Vesicle Size (nm)	Entrapment efficiency (%)
TE1	165.30±3.302	65.55±1.311
TE2	256.71±2.303	90.83±1.241
TE3	478.32±2.456	82.62±1.112

TE4	161.08±3.214	73.70±0.995
TE5	552.82±1.254	74.76±1.021
TE6	345.91±1.268	66.62±1.854
TE7	319.35±2.548	76.62±1.119
TE8	312.93±1.327	64.08±1.213

Among the formulations evaluated, TE4—prepared with elevated SPC and ethanol concentrations alongside a reduced level of propylene glycol—produced the smallest vesicle size and highest entrapment efficiency. Reducing SPC content was associated with an increase in vesicle size, as observed in TE5. Formulation TE8, containing low levels of both propylene glycol and ethanol, exhibited reduced entrapment efficiency.

Screening of influential formulation and process variables: The quality and performance of ethosomal formulations are governed by numerous formulation and process variables, making systematic evaluation through conventional one-factor-at-a-time approaches highly resource-intensive. In the present work, screening of relevant variables was conducted using a Taguchi L8 orthogonal array design at two levels for each of three factors. This experimental design minimized the total number of required runs during the initial screening phase, enabling identification of the most influential variables for subsequent optimization using a more detailed design of experiments (DOE) approach, particularly in cases where prior literature provided limited guidance on variable effects.

ANOVA was applied to the experimental data using Design Expert software to determine the coefficient estimates for the selected response variables. The results are presented in Table 5.9 and Figure 5.10.

Table 14: Data from design expert software for the coefficient of responses for independent factors

	Coefficient estimated	
Factors	**Vesicle Size(nm)**	**Entrapment Efficiency (%)**
Soya Phosphatidyl Choline	-84.3875	-5.61
Ethanol	53.83	1.3275
Propylene glycol	21.7875	-2.21

Evaluation of Vesicular Systems

Vesicle Size Determination

The vesicle size of the prepared ethosomal and liposomal formulations was determined using Dynamic Light Scattering (DLS) technique with the help of Malvern Zetasizer. The formulations were suitably diluted with distilled water to avoid multiple scattering effects and analyzed at room temperature.

Entrapment Efficiency

Entrapment efficiency of the vesicular formulations was determined by centrifugation method. The prepared vesicular dispersion was centrifuged at high speed to separate unentrapped drug from the vesicles. The supernatant containing free drug was collected, suitably diluted, and analyzedspectrophotometrically at the determined λmax using UV-visible spectrophotometer.

The percentage entrapment efficiency was calculated using the following equation:

$$EE\% = [[(Drug_{total} - Drug_{free})]/Drug_{total}] * 100$$

Transmission Electron Microscopy (TEM)

Morphological examination of optimized ethosomal and liposomal formulations was performed using Transmission Electron Microscopy (TEM). A drop of diluted vesicular dispersion was placed on carbon-coated copper grid and stained with phosphotungstic acid. Excess sample was removed and the grid was dried before analysis.

Optimization Validation Studies

Optimization studies were carried out using Design of Experiments (DoE) based Taguchi design. Response surface plots and feasibility analysis were used to evaluate the influence of independent variables such as phospholipid concentration and ethanol concentration on vesicle size and entrapment efficiency.

RESULTS AND DISCUSSION

Preformulation Studies

Organoleptic evaluation: Visual and sensory examination of the drug powder revealed that fluconazole presented as a white to off-white crystalline powder with no characteristic odor.

Table 15 Organoleptic property of fluconazole

Color	White to off white powder
Odor	Odorless
Taste	Tasteless

Determination of wavelength maxima in phosphate buffer pH 7.4: A UV spectrophotometric analytical method was developed for quantitative estimation of fluconazole, offering sensitivity, accuracy, and reproducibility. The method was designed to provide reliable and rapid determination of drug concentration.
UV absorption analysis of fluconazole in phosphate buffer pH 7.4 indicated maximum absorbance at 260 nm (Figure 5.1). A linear Beer-Lambert relationship was established with a correlation coefficient of 0.997 across a concentration range of 10–50 µg/ml. The three-dimensional absorption spectra are presented in Figure 5.2

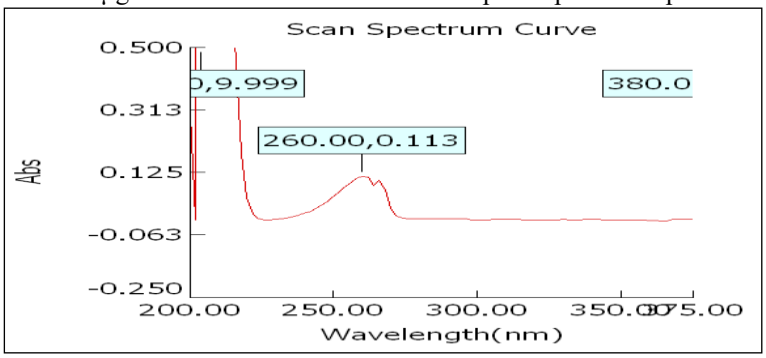

Figure 8 Wavelength maxima of fluconazole in phosphate buffer pH 7.4.

Determination of wavelength maxima in ethanol: The maximum UV absorbance of fluconazole dissolved in ethanol was observed at 260 nm (Figure 5.3). The drug exhibited a linear relationship between concentration and absorbance, with a correlation coefficient of 0.998 over the range of 10–50 µg/ml. Three-dimensional spectra in ethanol are illustrated in Figure 5.4

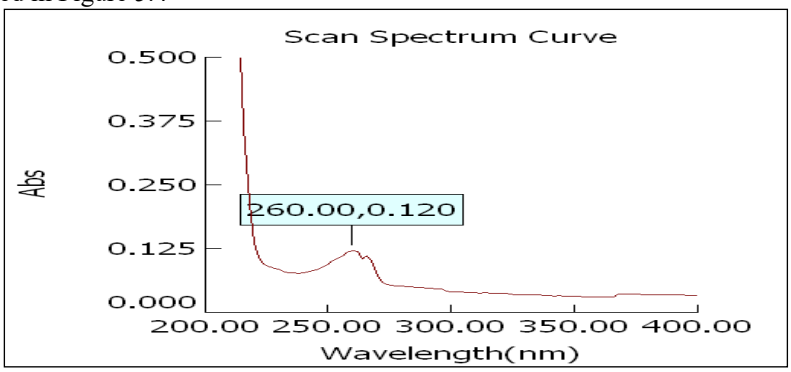

Figure 9: Wavelength maxima of fluconazole in ethanol

Calibration curve of fluconazole in phosphate buffer pH 7.4 and ethanol : Standard calibration curves were constructed by plotting absorbance against known drug concentrations. The regression coefficients (r^2) were determined to be 0.997 in phosphate buffer pH 7.4 and 0.998 in ethanol (Table 5.2), with statistical parameters detailed in Table 5.3. A linear concentration–absorbance relationship was confirmed over the range of 10–50 µg/ml in both media (Figures 5.5 and 5.6).

Table 16: Calibration curve points of the proposed method for the estimation of fluconazole.

Conc. (µg/ml)	Phosphate buffer pH 7.4 Absorbance* (260nm)	Ethanol Absorbance*(260nm)
10	0.110±0.002	0.075±0.001
20	0.210±0.001	0.169±0.002
30	0.325±0.002	0.281±0.001
40	0.425±0.001	0.398±0.002
50	0.556±0.001	0.510±0.001

*Average of three readings

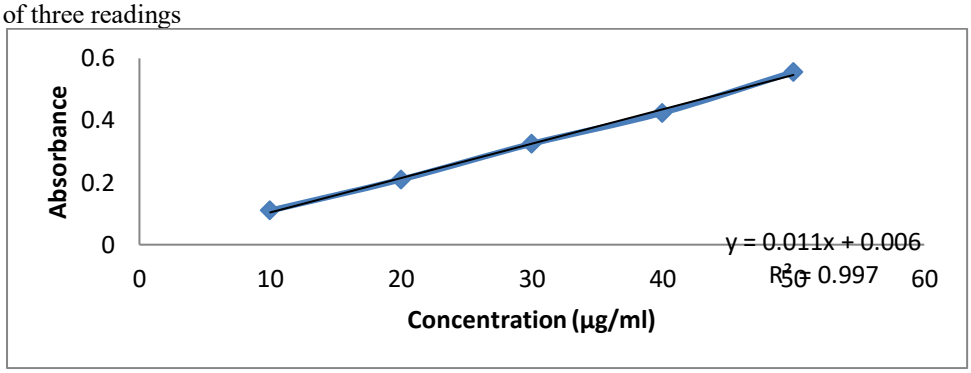

Figure 10: Calibration curve of fluconazole in phosphate buffer pH 7.4 at 260 nm

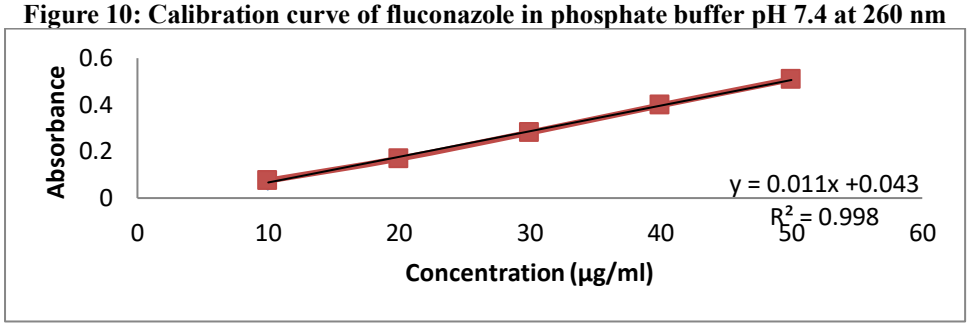

Figure 11: Calibration curve of fluconazole in ethanol at 260 nm

Table: 17: Statistical parameters related to standard curve of fluconazole at 260 nm

Media	Parameters	Values
Phosphate buffer pH 7.4	Beer's Law Range	10-50µg/ml
	Regression Coefficient	$R^2 = 0.997$
	Regressed line equation (y = mx + c)	y = 0.011x + 0.006
Ethanol	Beer's Law Range	10-50µg/ml
	Regression Coefficient	$R^2 = 0.998$
	Regressed line equation (y = mx + c)	y = 0.011x + 0.043

Where y is the response, x is the concentration, m is the slope and c is the intercept of a best fit line to the data.

Fourier-Transform Infra Red Spectroscopy (FTIR): The structural identity of the drug was confirmed through FTIR analysis. Diagnostic absorption peaks corresponding to the functional groups of fluconazole were identified and recorded. The characteristic peaks are depicted in Figure 5.7 and their corresponding wave numbers are listed in Table 5.4.

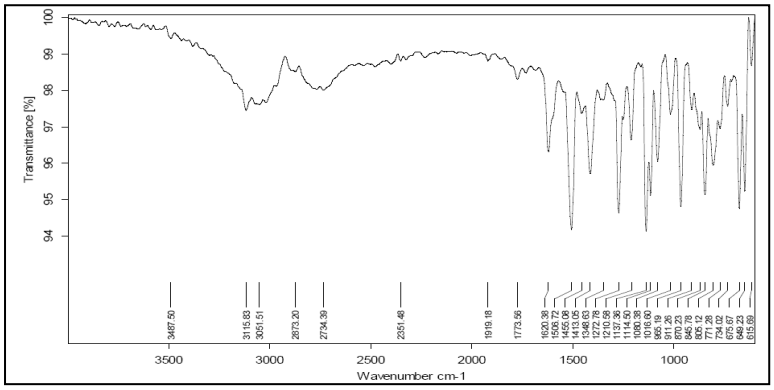

Figure 12: FT-IR of fluconazole

Table 18: Major peaks observed in the FTIR spectrum

Bands	Wave number(cm-1)
OH Streching	3487.50
CH2 Stretching	3115.83
C=C stretching vibration	1620.38
CH2 scissor stretching vibration	1413.05
C-C stretching vibration	1114.50
C - F Stretch	870.23

Changes in peak position or intensity in FTIR spectra are indicative of molecular interactions such as hydrogen bonding. The FTIR spectrum of fluconazole displayed a prominent absorption band at 3487.50 cm^{-1} attributable to O–H stretching, and a band at 3115.83 cm^{-1} corresponding to C–H stretching. In the 2,4-difluorobenzyl moiety, a C=C stretching vibration was observed at 1620.38 cm^{-1}. Additional peaks at 1413.05 cm^{-1} and 1114.50 cm^{-1} were assigned to CH_2 scissoring and C–C stretching vibrations, respectively.

Comparison of the obtained FTIR data with reference spectra from Sakharam et al. (2012) demonstrated agreement in the positions of functional group peaks, thereby confirming the purity and authenticity of the fluconazole sample.

Melting point determination: Melting point analysis serves as a primary indicator of sample purity, since even trace impurities can cause a measurable depression or broadening of the melting range. The experimentally determined melting point of fluconazole was 139°C (Figure 5.8), which is in conformity with Indian Pharmacopoeia standards and confirms the purity of the sample.

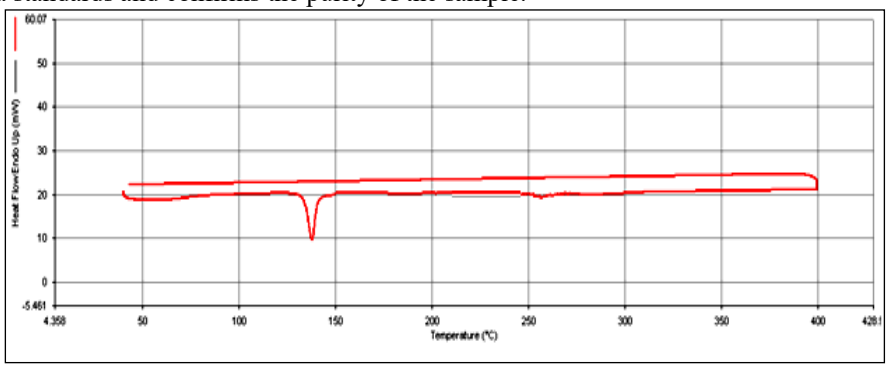

Figure 13: DSC thermogram showing melting point of fluconazole

pH of drug solution: The pH of a 1% w/v aqueous solution of fluconazole was measured using a calibrated digital pH meter and recorded as 7.8 ± 0.002

Flow properties: Bulk density, defined as the mass-to-volume ratio of a powder, is expressed in g/cm^3 and encompasses both the solid particle volume and interparticulate void space. This parameter is significant in the selection and sizing of processing and handling equipment (Jaimini et al., 2007). The measured flow properties of fluconazole API are presented in Table 5.5. A Carr's compressibility index of 53.30%, an angle of repose of 43.56°, and a Hausner's ratio of 1.5 were recorded, collectively indicating poor powder flowability and compressibility.

Table 19: Flow properties of fluconazole.

Parameter	Fluconazole
Angle of Repose	43.56o
Carr index (%)	53.30
Hausners Ratio	1.5

Solubility studies: The solubility profile of fluconazole was assessed in a range of solvents at ambient temperature (Table 5.6). The drug was found to be freely soluble in ethanol and methanol, soluble in DMSO, acetone, and chloroform, and slightly soluble in 0.1N hydrochloric acid and phosphate buffer pH 7.4. It was essentially insoluble in distilled water.

Table 20: Solubility studies of fluconazole in different solvent

Solvent used	Solubility(mg/ml)
Distilled Water	0.001±0.00

0.1 N Hydrochloric acid	11.12±0.22
Ethanol	63.25±0.54
Methanol	47.58±0.78
Chloroform	31.24±0.54
Acetone	21.57±0.43
DMSO	05.24±0.05
Citric acid buffer pH 1.2	30.21±0.54
Citric acid buffer pH 2.5	30.45±0.47
Acetic acid buffer pH 5.0	24.52±0.28
Phosphate buffer pH 7.4	35.24±0.34
Phosphate buffer pH 9.0	18.17±0.12
Phosphate buffer pH 10.0	15.95±0.04

Determination of partition coefficient: The partition coefficient was evaluated using the shake flask method to assess the relative distribution of the drug between aqueous and non-aqueous phases. This measurement facilitates the prediction of drug concentration in each phase. The partition coefficient of fluconazole was determined to be 0.57 ± 0.001, indicating its moderately hydrophobic character.

Loss on drying: The percentage of loss on drying of fluconazole was found to be 0.68±0.013% w/w respectively.

Drug-Excipient compatibility study: DSC analysis of fluconazole showed a characteristic endothermic peak at 139°C. Samples of the drug–cholesterol binary mixture stored under accelerated stability conditions (40°C/75% RH) for 30 days were subjected to DSC analysis. The melting endotherm of fluconazole remained unchanged at 139°C, indicating the absence of any physicochemical interaction between fluconazole and cholesterol (Figures 5.9–5.9c).

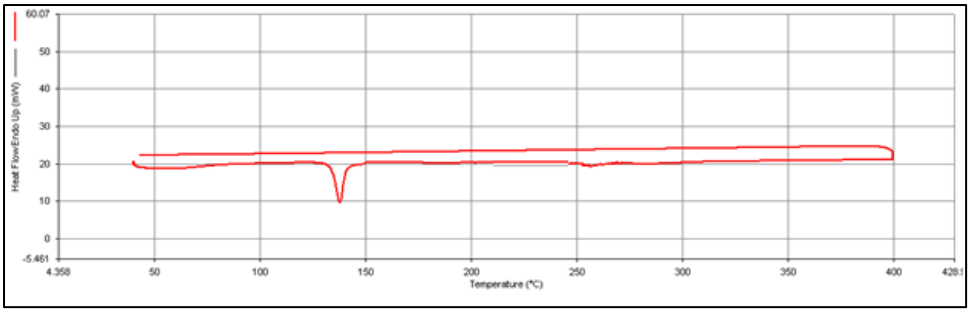

(a)

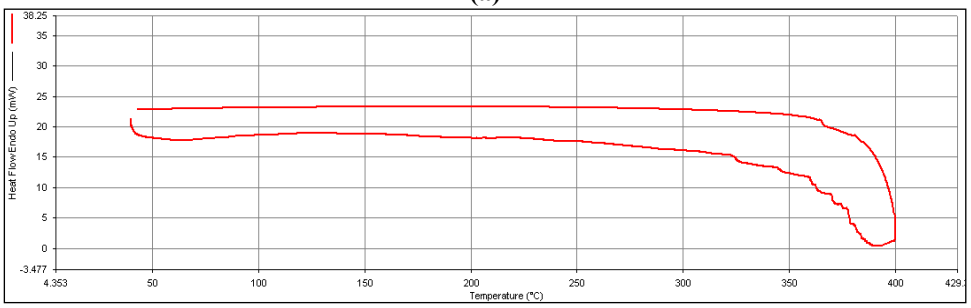

(b)

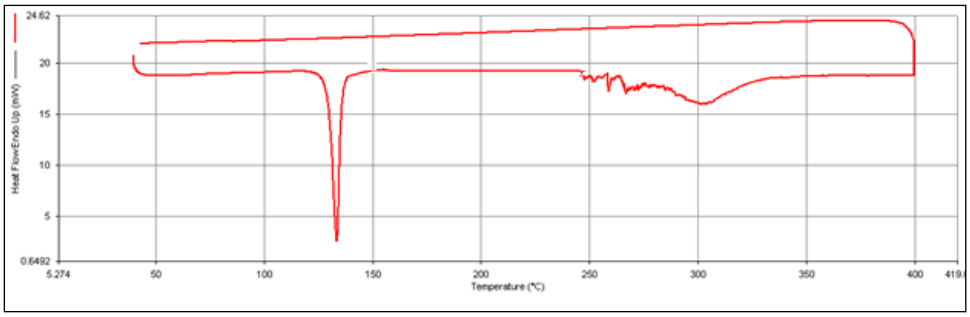

(c)

Figure 14: DSC thermogram of (a) pure drug, (b) cholesterol, (c) drug + cholesterol

Table 21: Comparative data of Preformulation studies

Parameter	Observation
Melting Point	139 ± 1.2oC
pH (1% w/v solution)	7.8±0.002
Angle of repose	43.56 Degree
Compressibility index (%)	53.30±0.05%.
Hausner ratio	1.5±0.001
Solubility of Fluconazole	Freely soluble in Ethanol, Methanol soluble in chloroform, slightly soluble in 0.1N HCl and insoluble in water
Partition coefficient	0.57±0.02
Loss on Drying (%)	0.68 ± 0.013

The results of preformulation characterization established that fluconazole is an odorless, white crystalline powder. The drug demonstrated solubility in phosphate buffer pH 7.4, acetone, and 0.1N HCl, with free solubility in methanol and ethanol, and negligible solubility in water. The experimentally determined melting point of 139 ± 2°C was consistent with the Indian Pharmacopoeia reference value of 140°C.

Analysis of the FTIR spectrum of the physical mixture confirmed that the characteristic functional groups of fluconazole were preserved, with no significant shifts or changes in peak intensities. This observation indicates that no chemical reaction occurred between the drug and cholesterol during preparation. DSC studies further corroborated compatibility between the two components. The partition coefficient value of 0.57 in an n-octanol/water system reflected the lipophilic tendency of fluconazole. Collectively, these preformulation data confirmed the feasibility of formulating fluconazole into ethosomal and liposomal vesicular drug delivery systems using appropriate preparation techniques.

Evaluation of Ethosomes: Table 5.8 summarizes vesicle size and entrapment efficiency data for the ethosomal formulations. Vesicle diameters ranged from 161.08 to 552.8 nm, while entrapment efficiency values spanned 63.70 to 90.89%.

Table 22: Evaluations of ethosomal formulations of Taguchi Screening Design

Formulation	Vesicle Size (nm)	Entrapment efficiency (%)
TE1	165.30±3.302	65.55±1.311
TE2	256.71±2.303	90.83±1.241
TE3	478.32±2.456	82.62±1.112
TE4	161.08±3.214	73.70±0.995
TE5	552.82±1.254	74.76±1.021
TE6	345.91±1.268	66.62±1.854
TE7	319.35±2.548	76.62±1.119
TE8	312.93±1.327	64.08±1.213

Among the formulations evaluated, TE4—prepared with elevated SPC and ethanol concentrations alongside a reduced level of propylene glycol—produced the smallest vesicle size and highest entrapment efficiency. Reducing SPC content was associated with an increase in vesicle size, as observed in TE5. Formulation TE8, containing low levels of both propylene glycol and ethanol, exhibited reduced entrapment efficiency.

Screening of influential formulation and process variables: The quality and performance of ethosomal formulations are governed by numerous formulation and process variables, making systematic evaluation through conventional one-factor-at-a-time approaches highly resource-intensive. In the present work, screening of relevant variables was conducted using a Taguchi L8 orthogonal array design at two levels for each of three factors. This

experimental design minimized the total number of required runs during the initial screening phase, enabling identification of the most influential variables for subsequent optimization using a more detailed design of experiments (DOE) approach, particularly in cases where prior literature provided limited guidance on variable effects.

ANOVA was applied to the experimental data using Design Expert software to determine the coefficient estimates for the selected response variables. The results are presented in Table 5.9 and Figure 5.10.

Table 23: Data from design expert software for the coefficient of responses for independent factors

Factors	Coefficient estimated	
	Vesicle Size(nm)	Entrapment Efficiency (%)
Soya Phosphatidyl Choline	-84.3875	-5.61
Ethanol	53.83	1.3275
Propylene glycol	21.7875	-2.21

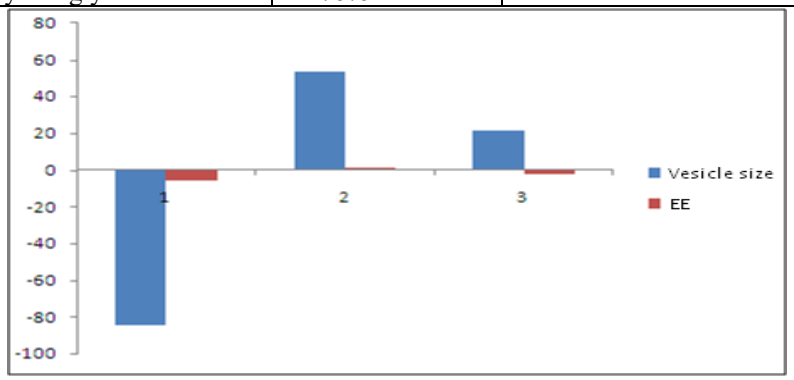

***1 SPC 2 Ethanol 3 Propylene Glycol**

Figure 15: Results for Taguchi design for selected response variables

Figure 15 illustrates the Taguchi design output for each measured response. The L8 array approach successfully identified the most impactful variables while minimizing experimental workload, thus conserving time and materials.

Higher SPC concentrations were associated with a reduction in both vesicle size and entrapment efficiency. In contrast, increasing the ethanol content resulted in a concurrent rise in vesicle size and entrapment efficiency.

Based on the magnitude of the estimated coefficients for vesicle size and entrapment efficiency, SPC (X1) and ethanol (X2) were identified as the primary influential factors for further optimization.

Model generation: The screening approach assumes approximate factor additivity and disregards interaction effects. Accordingly, a first-order L8 Taguchi design was applied, generating polynomial equations for vesicle size and entrapment efficiency (Equations 1–3). Seven regression coefficients (B1–B7) were estimated relative to the intercept B0.

$$Y=B0+B1X1+B2X2+B3X3+B4X4+B5X5+B6X6+B7X7 \quad (1)$$

$$\text{Vesicle Size} = 324.04+31.2+8.056+4.703448+31.85345+67+67.15+28.8 \ldots\ldots(2)$$

$$\text{Entrapment efficiency} = 73.097+1.625+1.46-6.13-3.425+3.5125+0.5875-2.5775 \ldots.(3)$$

Response surface plots: Three-dimensional response surface diagrams were constructed to visualize the individual and combined contributions of the selected variables on each measured response.

1. As illustrated in Figure 5.11, vesicle size diminished at low concentrations of both SPC and ethanol. A decrease was also noted at elevated SPC levels; however, increasing ethanol concentration led to a progressive increase in vesicle size. At intermediate SPC concentrations, a relative increase in vesicle size was observed.
2. Entrapment efficiency showed minimal variation at both low and high SPC concentrations. With increasing ethanol content, entrapment efficiency initially declined before recovering to higher values.
3. At elevated SPC combined with low ethanol levels, entrapment efficiency exhibited an initial increase followed by a decline. When ethanol concentration was high, entrapment efficiency showed a net increase, as

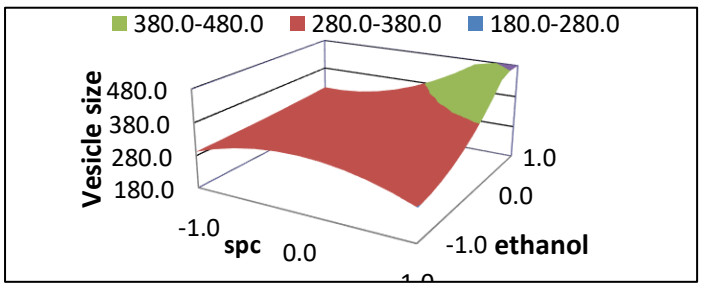

Figure 16: Response surface plot showing the influence SPC and ethanol on the value of vesicle size depicted in Figure 5.12.

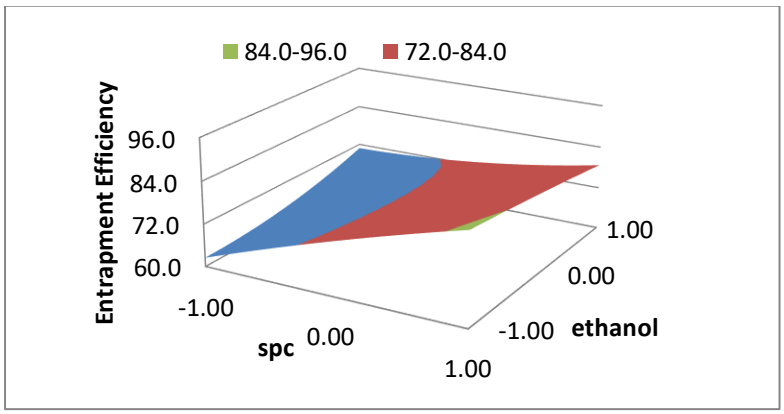

Figure 17: Response surface plot showing the influence SPC and ethanol on the value of entrapment efficiency

Table 24: Feasibility search for vesicle size (<340) Minimum: 292.4, Maximum: 347.8nm

	-1.0	-0.8	-0.6	-0.4	-0.2	0.0	0.2	0.4	0.6	0.8	1.0
-1.0	292.4	313.5	329.6	340.7	346.7	347.8	343.9	335.1	321.2	302.3	278.4
-0.8	292.9	309.8	322.7	331.7	336.8	338.0	335.2	328.6	318.0	303.4	285.0
-0.6	293.7	306.8	317.0	324.4	329.0	330.7	329.5	325.5	318.7	309.0	296.5
-0.4	294.8	304.5	312.5	318.8	323.2	325.9	326.8	326.0	323.3	318.9	312.8
-0.2	296.0	303.0	309.2	314.7	319.6	323.7	327.1	329.9	331.9	333.3	333.9
0.0	297.5	302.1	307.0	312.3	318.0	324.0	330.5	337.3	344.5	352.0	359.9
0.2	299.3	301.9	306.0	311.5	318.5	326.9	336.8	348.1	360.9	375.1	390.8
0.4	301.3	302.5	306.2	312.4	321.1	332.4	346.1	362.4	381.3	402.6	426.5
0.6	303.6	303.7	307.5	314.8	325.8	340.3	358.5	380.2	405.6	434.5	467.1
0.8	306.1	305.7	310.0	318.9	332.6	350.9	373.8	401.5	433.8	470.8	512.5
1.0	308.8	308.3	313.6	324.6	341.4	363.9	392.2	426.2	466.0	511.5	562.8

SPC and ethanol were taken forward as the two key variables for optimization. As shown in Table 24, a feasibility search for vesicle size identified a region satisfying the target criterion (vesicle size < 340 nm). This region corresponded to ethanol levels of 0.6 to 1.0 and SPC levels of −1.0 to −0.6, which were then used to define the boundaries for intensive grid searching

Table 25: Feasibility search for entrapment efficiency (>75%) Minimum: 62.5, Maximum: 85.7%

	-1.00	-0.80	-0.60	-0.40	-0.20	0.00	0.20	0.40	0.60	0.80	1.00
-1.00	62.5	65.1	67.7	70.2	72.6	74.9	77.2	79.4	81.6	83.7	85.7
-0.80	62.6	65.1	67.5	69.8	72.2	74.4	76.7	78.8	81.0	83.1	85.1
-0.60	62.9	65.2	67.4	69.6	71.8	74.0	76.1	78.3	80.4	82.4	84.5
-0.40	63.3	65.4	67.5	69.5	71.6	73.6	75.7	77.7	79.8	81.8	83.8
-0.20	63.9	65.8	67.6	69.5	71.4	73.3	75.3	77.2	79.2	81.2	83.1
0.00	64.7	66.3	67.9	69.6	71.3	73.1	74.9	76.7	78.6	80.5	82.5
0.20	65.6	66.9	68.3	69.8	71.3	72.9	74.6	76.3	78.0	79.9	81.7
0.40	66.6	67.7	68.9	70.1	71.4	72.8	74.3	75.9	77.5	79.2	81.0
0.60	67.9	68.7	69.6	70.5	71.6	72.8	74.1	75.5	77.0	78.6	80.2
0.80	69.3	69.7	70.3	71.1	71.9	72.9	73.9	75.1	76.5	77.9	79.5
1.00	70.8	71.0	71.3	71.7	72.3	73.0	73.8	74.8	76.0	77.2	78.7

The feasibility analysis for entrapment efficiency (Table 25) identified a suitable region meeting the target threshold (> 75%). This region aligned with the same boundary conditions—ethanol levels of 0.6 to 1.0 and SPC levels of −1.0 to −0.6—confirming their suitability for the intensive grid search.

Intensive grid search for locating a region of optimized formulation

Table 26: Intensive grid search for vesicle size

	0.6	0.64	0.68	0.72	0.76	0.8	0.84	0.88	0.92	0.96	0.1

0	344.5	345.9	347.4	348.9	350.5	352.0	353.6	355.1	356.7	358.3	327.2
0.04	347.4	349.2	350.9	352.7	354.5	356.3	358.1	360.0	361.9	363.8	327.9
0.08	350.6	352.5	354.5	356.6	358.6	360.7	362.9	365.0	367.2	369.4	328.7
0.12	353.9	356.1	358.3	360.6	363.0	365.4	367.8	370.2	372.7	375.3	329.6
0.16	357.3	359.8	362.3	364.9	367.5	370.2	372.9	375.6	378.5	381.3	330.6
0.2	360.9	363.6	366.4	369.3	372.2	375.1	378.2	381.2	384.4	387.6	331.7
0.24	364.7	367.7	370.7	373.8	377.0	380.3	383.6	387.0	390.5	394.0	332.9
0.28	368.6	371.8	375.2	378.6	382.1	385.6	389.2	392.9	396.7	400.6	334.2
0.32	372.7	376.2	379.8	383.5	387.3	391.1	395.1	399.1	403.2	407.4	335.7
0.36	376.9	380.7	384.6	388.6	392.6	396.8	401.0	405.4	409.8	414.4	337.3
0.4	381.3	385.4	389.5	393.8	398.2	402.6	407.2	411.9	416.7	421.5	338.9

Based on the intensive grid search data in Table 26, three formulation compositions were identified with predicted responses meeting the required specifications. These were subsequently prepared and evaluated experimentally to verify the predicted outcomes. The same coordinates were used for the entrapment efficiency grid search. The three selected points corresponded to: SPC at level 0/ethanol at 0.6; SPC at 0.16/ethanol at 0.76; and SPC at 0/ethanol at 0.96.

Table 27: Intensive grid search for entrapment efficiency

	0.6	0.64	0.68	0.72	0.76	0.8	0.84	0.88	0.92	0.96	0.1
0	84.8	85.2	85.5	85.9	86.3	86.7	87.1	87.5	87.8	88.2	80.2
0.04	84.7	85.0	85.4	85.8	86.2	86.6	86.9	87.3	87.7	88.1	80.1
0.08	84.6	84.9	85.3	85.7	86.0	86.4	86.8	87.2	87.6	88.0	80.1
0.12	84.4	84.8	85.2	85.5	85.9	86.3	86.7	87.1	87.4	87.8	80.0
0.16	84.3	84.7	85.1	85.4	85.8	86.2	86.5	86.9	87.3	87.7	80.0
0.2	84.2	84.6	84.9	85.3	85.7	86.0	86.4	86.8	87.2	87.5	79.9
0.24	84.1	84.5	84.8	85.2	85.5	85.9	86.3	86.6	87.0	87.4	79.9
0.28	84.0	84.4	84.7	85.1	85.4	85.8	86.1	86.5	86.9	87.2	79.8
0.32	83.9	84.2	84.6	84.9	85.3	85.6	86.0	86.4	86.7	87.1	79.8
0.36	83.8	84.1	84.5	84.8	85.2	85.5	85.9	86.2	86.6	87.0	79.8
0.4	83.7	84.0	84.4	84.7	85.0	85.4	85.7	86.1	86.5	86.8	79.7

Following the same approach as for vesicle size, three candidate formulations were identified from Table 5.13 for entrapment efficiency. These included SPC at level 0 with ethanol at 0.6, SPC at 0.16 with ethanol at 0.76, and SPC at 0 with ethanol at 0.96. The predicted responses were confirmed by experimental evaluation.

Experimental results with predicted responses: Following DOE analysis, formulation EF2 was selected as the optimized ethosomal formulation for incorporation into the gel base. This selection was based on the close agreement between experimental and predicted response values, and the fact that all observed parameters were within acceptable limits.

Table 28: Experimental results with predicted responses

Formulation	Composition SPC/ Ethanol	Response	Predicted value	Experimental value
EF1	3/43	Vesicle size	344.5	341.1
		Entrapment efficiency (%)	84.8	82.19
EF2	3.40/46.40	Vesicle size	367.5	368.4
		Entrapment efficiency (%)	85.8	85.50
EF3	3/49.40	Vesicle size	358.3	364.4
		Entrapment efficiency (%)	88.2	81.91

*Formulation EF2 selected as optimized formulation

Evaluation of Liposomes: Table 29 presents vesicle size and entrapment efficiency data for all liposomal batches. Particle sizes ranged from 126.79 to 510.13 nm, and entrapment efficiency values varied between 59.50 and 91.70%.

Table 29: Evaluation of liposomal formulations of Taguchi Screening Design

Formulation	Vesicle Size (nm)	Entrapment efficiency (%)
TL1	127.95±2.421	76.53±1.530
TL2	290.50±2.112	82.75±1.235
TL3	338.24±1.198	55.12±1.241
TL4	126.79±1.175	66.71±1.021
TL5	510.13±1.154	82.12±1.118
TL6	200.06±1.256	91.70±1.029
TL7	183.89±2.014	59.50±1.147

TL8	347.84±1.997	73.12±1.124

The screening results indicated that formulation TL6, prepared at elevated lecithin and cholesterol levels, yielded smaller vesicles with higher entrapment efficiency. Conversely, increasing cholesterol concentration alone was associated with reductions in both vesicle size and entrapment efficiency.

Screening of influential formulation and process variables: Liposomal performance is sensitive to a range of formulation and process parameters, and their simultaneous evaluation through traditional approaches is impractical. A Taguchi L8 orthogonal array design was therefore applied to screen three factors at two levels, allowing efficient identification of the most critical variables with a reduced experimental burden, in preparation for detailed DOE optimization. The experimental screening was designed to require the minimum number of runs, with a focus on identifying variables for which limited published data were available.

ANOVA was performed on the evaluation data using Design Expert software, and the resulting coefficient estimates for the response variables are reported in Table 5.16.

Table 30: Data from design expert software for the coefficient of responses for independent factors

	Coefficient estimated	
Factors	Vesicle Size (nm)	Entrapment efficiency (%)
SPC	-10.1625	4.025
Cholestrol	24.0925	-7.575
Speed	1.8275	-3.575

The Taguchi design outputs for liposomal response variables are shown in Figure 30. The L8 array strategy efficiently identified the key formulation variables with minimal experimental runs, thereby reducing expenditure of time, effort, and materials.

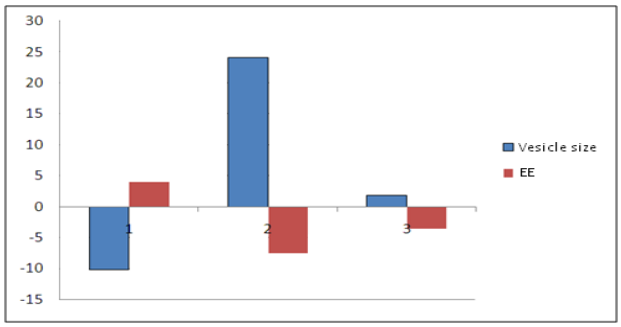

***1 SPC 2 Cholesterol 3 Speed**

Figure 18: Results for Taguchi design for selected response variables

Higher cholesterol content was associated with reduced entrapment efficiency and an increase in vesicle size. Increasing SPC concentration, conversely, produced smaller vesicles and improved entrapment efficiency. Analysis of the coefficient magnitudes for both response variables confirmed that SPC (X1) and cholesterol (X2) were the most influential factors and were selected for further optimization.

Model Generation: Consistent with the assumptions of factor additivity and minimal interactions inherent in screening designs, a first-order polynomial model was generated using the L8 Taguchi framework. The resulting equations for vesicle size and entrapment efficiency (Equations 4–6) incorporated seven regression coefficients (B1–B7) relative to intercept B0, as expressed in the general polynomial equation.

$$Y=B0+B1X1+B2X2+B3X3+B4X4+B5X5+B6X6+B7X7 \quad (4)$$

$$\text{Vesicle Size} = 265.67+31.2+8.056+4.703448+31.85345+67+67.15+28.8 \quad (5)$$

$$\text{Entrapment efficiency} =73.425+1.625+1.46-6.13-3.425+3.5125+0.5875-2.5775 \quad (6)$$

Response surface plots: Response surface diagrams were generated to provide a visual representation of the effects of lecithin and cholesterol on the formulation responses, enabling intuitive assessment of variable contributions and their interactions.

1. As depicted in Figure 5.14, vesicle size reached its maximum at intermediate lecithin concentrations and declined at high lecithin levels under conditions of low cholesterol. At elevated cholesterol concentrations, the rate of increase in vesicle size was more pronounced.
2. Entrapment efficiency remained relatively stable at both extremes of lecithin concentration. Under low cholesterol conditions, a biphasic response was observed, with an initial decline followed by an improvement in entrapment efficiency.
3. Figure 5.15 illustrates that entrapment efficiency initially rose and subsequently declined with increasing lecithin concentration when cholesterol levels were low. Higher cholesterol concentrations were consistently associated with improved entrapment efficiency.

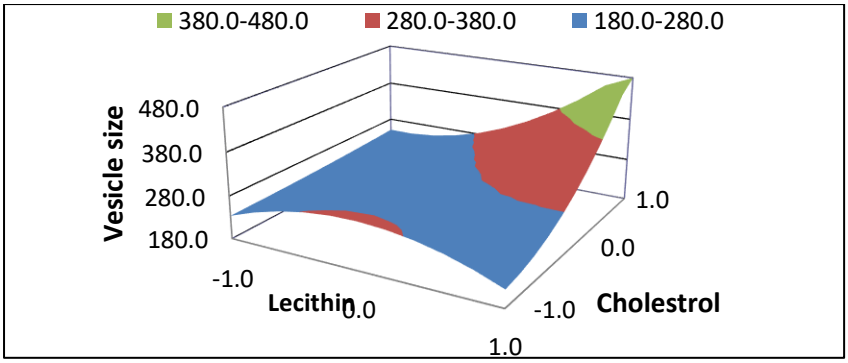

Figure 19: Response surface plot showing the influence lecithin and cholesterol on the value of vesicle size

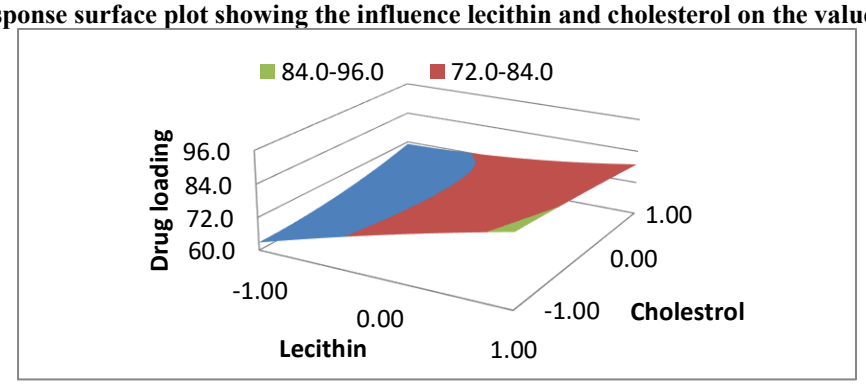

Figure 20: Response surface plot showing the influence lecithin and cholesterol on the value of entrapment efficiency

Table 31: Feasibility search for vesicle size (vesicle size <280nm Min 220nm Max 289.5nm)

	-1.0	-0.8	-0.6	-0.4	-0.2	0.0	0.2	0.4	0.6	0.8	1.0
-1.0	234.0	255.1	271.2	282.3	288.4	289.5	285.6	276.7	262.8	243.9	220.0
-0.8	234.6	251.4	264.4	273.4	278.4	279.6	276.9	270.2	259.6	245.1	226.6
-0.6	235.4	248.4	258.7	266.1	270.6	272.3	271.2	267.2	260.3	250.6	238.1
-0.4	236.4	246.2	254.2	260.4	264.9	267.5	268.5	267.6	265.0	260.6	254.4
-0.2	237.7	244.6	250.8	256.4	261.2	265.3	268.8	271.5	273.6	274.9	275.6
0.0	239.2	243.7	248.6	253.9	259.6	265.7	272.1	278.9	286.1	293.6	301.6
0.2	240.9	243.6	247.6	253.2	260.1	268.6	278.4	289.8	302.5	316.8	332.4
0.4	242.9	244.1	247.8	254.0	262.7	274.0	287.8	304.1	322.9	344.3	368.2
0.6	245.2	245.3	249.1	256.5	267.4	282.0	300.1	321.9	347.2	376.2	408.7
0.8	247.7	247.3	251.6	260.6	274.2	292.5	315.5	343.1	375.5	412.5	454.2
1.0	250.4	250.0	255.2	266.3	283.0	305.6	333.8	367.9	407.6	453.2	504.4

Table 31 presents the feasibility search for vesicle size. The region satisfying the specification (vesicle size < 280 nm) was identified at cholesterol levels of 0.6 to 1.0 combined with lecithin levels of −1.0 to −0.6, which were used to define the intensive grid search domain.

Table 32: Feasibility search for vesicle size entrapment efficiency >75%(Min 62.8% Max 86.0%)

	-1.00	-0.80	-0.60	-0.40	-0.20	0.00	0.20	0.40	0.60	0.80	1.00
-1.00	62.8	65.4	68.0	70.5	72.9	75.3	77.5	79.8	81.9	84.0	86.0
-0.80	62.9	65.4	67.8	70.2	72.5	74.8	77.0	79.2	81.3	83.4	85.4
-0.60	63.2	65.5	67.7	70.0	72.2	74.3	76.5	78.6	80.7	82.7	84.8

-0.40	63.6	65.7	67.8	69.8	71.9	74.0	76.0	78.0	80.1	82.1	84.1
-0.20	64.2	66.1	68.0	69.8	71.7	73.7	75.6	77.5	79.5	81.5	83.5
0.00	65.0	66.6	68.3	69.9	71.7	73.4	75.2	77.1	78.9	80.8	82.8
0.20	65.9	67.3	68.7	70.1	71.7	73.3	74.9	76.6	78.4	80.2	82.1
0.40	67.0	68.1	69.2	70.5	71.8	73.2	74.6	76.2	77.8	79.5	81.3
0.60	68.2	69.0	69.9	70.9	72.0	73.1	74.4	75.8	77.3	78.9	80.6
0.80	69.6	70.1	70.7	71.4	72.2	73.2	74.3	75.5	76.8	78.2	79.8
1.00	71.1	71.3	71.6	72.0	72.6	73.3	74.2	75.2	76.3	77.6	79.0

The feasibility search for entrapment efficiency (Table 32) identified the favorable region meeting the threshold of > 75% within the same parameter space: cholesterol levels of 0.6 to 1.0 and lecithin levels of −1.0 to −0.6, consistent with the vesicle size search region.

Intensive grid search for locating a region of optimized formulation

Table 33: Intensive grid search for vesicle size

	0.6	0.64	0.68	0.72	0.76	0.8	0.84	0.88	0.92	0.96	0.1
0	286.1	287.6	289.1	290.6	292.1	293.6	295.2	296.8	298.4	300.0	268.8
0.04	289.1	290.8	292.5	294.3	296.1	297.9	299.8	301.6	303.5	305.4	269.5
0.08	292.2	294.2	296.2	298.2	300.3	302.4	304.5	306.7	308.9	311.1	270.3
0.12	295.5	297.7	300.0	302.3	304.6	307.0	309.4	311.9	314.4	316.9	271.2
0.16	298.9	301.4	303.9	306.5	309.1	311.8	314.5	317.3	320.1	323.0	272.2
0.2	302.5	305.3	308.1	310.9	313.8	316.8	319.8	322.9	326.0	329.2	273.3
0.24	306.3	309.3	312.3	315.5	318.7	321.9	325.2	328.6	332.1	335.6	274.5
0.28	310.2	313.5	316.8	320.2	323.7	327.2	330.9	334.6	338.4	342.2	275.9
0.32	314.3	317.8	321.4	325.1	328.9	332.7	336.7	340.7	344.8	349.0	277.3
0.36	318.5	322.3	326.2	330.2	334.3	338.4	342.7	347.0	351.5	356.0	278.9
0.4	322.9	327.0	331.2	335.4	339.8	344.3	348.8	353.5	358.3	363.2	280.6

The favorable region was further subdivided for the intensive grid search (Table 5.19). Three formulation compositions with promising predicted vesicle sizes were selected and experimentally validated. The same compositions were evaluated for entrapment efficiency. The selected points corresponded to: cholesterol at 0.76/lecithin at 0.16; cholesterol at 0.84/lecithin at 0.04; and cholesterol at 0.96/lecithin at 0.

Table 34: Intensive grid search for entrapment efficiency

	0.6	0.64	0.68	0.72	0.76	0.8	0.84	0.88	0.92	0.96	0.1
0	78.9	79.3	79.7	80.1	80.5	80.8	81.2	81.6	82.0	82.4	74.3
0.04	78.8	79.2	79.6	79.9	80.3	80.7	81.1	81.5	81.9	82.2	74.3
0.08	78.7	79.1	79.4	79.8	80.2	80.6	81.0	81.3	81.7	82.1	74.2
0.12	78.6	79.0	79.3	79.7	80.1	80.4	80.8	81.2	81.6	82.0	74.2
0.16	78.5	78.8	79.2	79.6	79.9	80.3	80.7	81.1	81.4	81.8	74.1
0.2	78.4	78.7	79.1	79.5	79.8	80.2	80.6	80.9	81.3	81.7	74.1
0.24	78.3	78.6	79.0	79.3	79.7	80.1	80.4	80.8	81.2	81.5	74.0
0.28	78.2	78.5	78.9	79.2	79.6	79.9	80.3	80.7	81.0	81.4	74.0
0.32	78.0	78.4	78.7	79.1	79.4	79.8	80.2	80.5	80.9	81.3	74.0
0.36	77.9	78.3	78.6	79.0	79.3	79.7	80.0	80.4	80.7	81.1	73.9

0.4	77.8	78.2	78.5	78.8	79.2	79.5	79.9	80.2	80.6	81.0	73.9

Three formulations were shortlisted from Table 34 based on predicted entrapment efficiency values. These were: cholesterol at level 0 with lecithin at 0.96; cholesterol at 0.04 with lecithin at 0.84; and cholesterol at 0.16 with lecithin at 0.76. Experimental results were compared against predicted values to verify model accuracy

Experimental results with predicted responses: Based on DOE analysis, formulation LF3 was identified as the optimized liposomal formulation for gel preparation. Experimental response values showed satisfactory agreement with model predictions, and all parameters were within the defined specification limits.

Table 35: Experimental results with predicted responses

Formulation	Composition Lecithin/ Cholesterol	Response	Predicted value	Experimental value
LF1	158/37.6	Vesicle size	309.10	321.1
		Entrapment efficiency(%)	79.90	76.19
LF2	152/38.4	Vesicle size	299.80	258.4
		Entrapment efficiency(%)	81.10	75.50
LF3	150/39.6	Vesicle size	300.0	320.4
		Entrapment efficiency(%)	82.40	76.91

CONCLUSION

The present investigation successfully established the feasibility of developing fluconazole-loaded ethosomal and liposomal vesicular systems for enhanced topical/transdermal delivery. Comprehensive preformulation studies confirmed the identity, purity, and suitability of fluconazole for vesicular formulation development. The drug exhibited characteristic organoleptic properties, acceptable melting point, and distinctive FTIR peaks corresponding to its functional groups. DSC and FTIR compatibility studies demonstrated the absence of any significant physicochemical interaction between fluconazole and cholesterol, confirming compatibility of the selected excipients.

Solubility and partition coefficient studies revealed the moderately lipophilic nature of fluconazole, supporting its suitability for incorporation into lipid-based vesicular carriers. Flow property analysis indicated poor powder flowability, emphasizing the need for specialized formulation approaches to improve drug delivery performance.

Ethosomal formulations prepared using the Taguchi screening design demonstrated vesicle sizes ranging from 161.08 to 552.82 nm and entrapment efficiencies between 63.70% and 90.83%. Statistical optimization identified soya phosphatidylcholine (SPC) and ethanol concentration as the most influential formulation variables affecting vesicle size and drug entrapment. Through feasibility and intensive grid search analysis, formulation EF2 was identified as the optimized ethosomal formulation, exhibiting close agreement between predicted and experimental responses with satisfactory vesicle size and high entrapment efficiency.

Similarly, liposomal formulations showed vesicle sizes ranging from 126.79 to 510.13 nm with entrapment efficiencies between 55.12% and 91.70%. Optimization studies confirmed lecithin and cholesterol concentration as the critical factors influencing liposomal characteristics. Among the prepared batches, formulation LF3 was selected as the optimized liposomal formulation based on acceptable experimental responses and satisfactory agreement with predicted values.

The Taguchi L8 orthogonal array design proved to be an efficient and economical approach for screening and optimization of formulation variables while minimizing the number of experimental runs. Response surface analysis and feasibility studies successfully identified optimized formulation regions for both vesicular systems.

Overall, the findings of the study demonstrate that both ethosomal and liposomal carriers are promising vesicular systems for the delivery of fluconazole. The optimized formulations exhibited desirable vesicle size, high entrapment efficiency, and good physicochemical stability, indicating their potential for improved topical/transdermal antifungal therapy. These vesicular systems may enhance drug penetration, improve therapeutic efficacy, reduce systemic side effects, and provide a more effective alternative to conventional fluconazole formulations.

REFERENCES

1. Allen, T. M., & Cullis, P. R. (2013). Liposomal drug delivery systems: From concept to clinical applications. Advanced Drug Delivery Reviews, 65(1), 36–48. https://doi.org/10.1016/j.addr.2012.09.037

2. Benech, R. O., Kheadr, E. E., Laridi, R., & Lacroix, C. (2002). Liposomes as carriers for the food industry. Journal of Food Protection, 65(12), 1929–1940.

3. Gabizon, A., Shmeeda, H., &Barenholz, Y. (2003). Pharmacokinetics of pegylated liposomal doxorubicin. Clinical Pharmacokinetics, 42(5), 419–436.

4. Gabizon, A., Catane, R., Uziely, B., Kaufman, B., Safra, T., Cohen, R., …Barenholz, Y. (1998). Prolonged circulation time of liposomes. Cancer Research, 58(14), 331–335.

5. Jain, N. K., Mishra, V., & Mehra, N. K. (2004). Targeted drug delivery to macrophages. Journal of Pharmacy and Pharmacology, 56(4), 443–452.

6. Jain, S., Tiwary, A. K., Sapra, B., & Jain, N. K. (2007). Formulation and evaluation of ethosomes. Journal of Controlled Release, 110(2), 296–303.

7. Kumar, R., Philip, A., & Pathak, K. (2007). Development and evaluation of transdermal drug delivery systems. International Journal of Pharmaceutical Sciences, 69(1), 1–10.

8. Chavan, A., Daniel, K., & Patel, A. M. (2022). In-silico Exploration of Phytoconstituents of Gymnema sylvestre as Potential Glucokinase Activators and DPP-IV Inhibitors for the Future Synthesis of Silver Nanoparticles for the Treatment of Type 2 Diabetes Mellitus. Current Enzyme Inhibition, 18(1), 47-60.

9. Kumar, S., Kamboj, S., & Saini, V. (2004). Transdermal drug delivery system: A review. International Journal of Pharmaceutical Sciences Review and Research, 5(2), 35–45.

10. Manosroi, A., Jantrawut, P., &Manosroi, J. (2009). Novel ethosomes for transdermal delivery. Drug Delivery, 16(6), 316–322.

11. Sheehan, D. J., Hitchcock, C. A., & Sibley, C. M. (1999). Current and emerging azole antifungal agents. Clinical Microbiology Reviews, 12(1), 40–79.

12. Singh, B., Dahiya, M., Saharan, V., & Ahuja, N. (2005). Optimization techniques in pharmaceutical formulation. Drug Development and Industrial Pharmacy, 31(8), 761–775.

13. Singh, B., Kumar, R., & Ahuja, N. (2006). Response surface methodology in drug delivery. Critical Reviews in Therapeutic Drug Carrier Systems, 23(1), 27–105.

14. Sobel, J. D. (2007). Vulvovaginalcandidosis. The Lancet, 369(9577), 1961–1971.

15. Touitou, E., Dayan, N., Bergelson, L., Godin, B., & Eliaz, M. (2000). Ethosomes—novel vesicular carriers. Journal of Controlled Release, 65(3), 403–418.

16. Verma, P., & Pathak, K. (2010). Therapeutic and cosmeceutical potential of ethosomes. Journal of Advanced Pharmaceutical Technology & Research, 1(3), 274–282.

.